OPTIMIZATION OF SUPERHYDROPHOBIC SURFACES TO MAINTAIN CONTINUOUS DROPWISE CONDENSATION

Aref Vandadi

Thesis Prepared for the Degree of

MASTER OF SCIENCE

UNIVERSITY OF NORTH TEXAS

May 2014

APPROVED:

Jiangtao Cheng, Major Professor
Sheldon Shi, Committee Member
Xu Nie, Committee Member
Yong Tao, Chair of the Department of Mechanical and Energy Engineering
Costas Tsatsoulis, Dean of the College of Engineering
Mark Wardell, Dean of the Toulouse Graduate School

Vandadi, Aref. Optimization of superhydrophobic surfaces to maintain continuous dropwise condensation. Master of Science (Mechanical and Energy Engineering), May 2014, 43 pp., 29 figures, 44 numbered references.

In the past decade, the condensation on superhydrophobic surfaces has been investigated abundantly to achieve dropwise condensation. There is not a specific approach in choosing the size of the roughness of the superhydrophobic surfaces and it was mostly selected arbitrarily to investigate the behavior of condensates on these surfaces. In this research, we are optimizing the size of the roughness of the superhydrophobic surface in order to achieve dropwise condensation. By minimizing the resistances toward the transition of the tails of droplets from the cavities of the roughness to the top of the roughness, the size of the roughness is optimized. It is shown that by decreasing the size of the roughness of the superhydrophobic surface, the resistances toward the transition of the tails of droplets from Wenzel state to Cassie state decrease and consequently dropwise condensation becomes more likely.

ACKNOWLEDGEMENTS

Foremost, I would like to extend my deep gratitude to my advisor Dr. Jiangtao Cheng for his guidance, encouragement and continued support during my master's degree. I couldn't have imagined having a better advisor for my master study.

I also want to thank my friends, my parents, my brother and his wife for helping me to get over the hardships that I went through during the past 2 years. They were a great support in all my struggles in my new life and study in this country.

TABLE OF CONTENTS

Page

LIST OF FIGURES

Page

CHAPTER 1

INTRODUCTION

In the past decade there have been numerous researches on condensation on superhydrophobic surfaces. The ability of these surfaces in providing a bare surface during condensation has attracted many researchers to exploit this potential in order to enhance phase change heat transfer of water vapor. Due to the low surface energy and the roughness, drops are mobile on these surfaces and could be removed easily even in the absence of the effect of gravity which would provide bare surfaces leading to continuous condensation.

Dropwise condensation was first discovered about 80 years ago [1]. There has been a large amount of research in developing various hydrophobic surfaces using different nonwetting coatings in order to enhance dropwise condensation. As a result of recent progress in nanofabrication, superhydrophobic surfaces were introduced on which water droplets have high contact angles and significant mobility. Micro/nano-structures of the surface are an essential part of superhydrophobic surfaces in order to induce high water repellency. The high water repellency of superhydrophobic surfaces has attracted many researchers to exploit this potential during condensation of water vapor in order to improve heat transfer. Different characteristics of on structured surfaces when confronted with water through deposition or condensation such as the invasion of water into structures, consequent states of drops and the growth of drops during condensation were abundantly studied [2-6]. Continuous dropwise condensation in the absence of external force was first reported by Boreyko and Chen [7]. They captured droplet jumping as a result of coalescence during condensation on

superhydrophobic surfaces and mentioned that coalescence-induced jumping could lead to an autonomous droplet removal and consequently might enhance condensation heat transfer. Wang et al. [8] proposed an analytical relation to examine the effect of droplet size on coalescence-induced velocity considering viscous dissipation. Liu et al. [9] also did a more comprehensive analysis on coalescence of drops considering viscous dissipation, gravity and work of adhesion. Different events as a result of coalescence-induced jumping were reported such as serial coalescence events [10] and continuous jumping relay [11] which lead to removing the drops from the surface in the absence of any external forces. Chen et al. [12] used local wettable nucleation sites on a hierarchical surface and reported an increase in drop number density and droplet self-removal volume compared to superhydrophobic surfaces with nanostructures alone. Ma et al. [13] investigated the effect of noncondensable gas on dropwise condensation characteristics. They mentioned that by increasing the concentration of noncondensable gas, drops formed on superhydrophobic surface during condensation would transition from Wenzel state to Cassie. Cheng et al. [14] studied condensation on hierarchical superhydrophobic surfaces in environmental scanning electron microscope (ESEM) and vapor chamber. Continuous dropwise condensation in ESEM and a film layer of condensate in vapor chamber were observed. They reported that heat transfer coefficient is lower on superhydrophobic surface than hydrophobic smooth surface in vapor chamber. Miljkovic et al. [15] demonstrated a higher heat flux and higher condensation heat transfer coefficient during condensation on nano-textured copper surface at low super-saturations. The effect of nano-roughness on the dynamics of condensed micro-drops was studied by Rykaczewski et al. [16]. They defined a

volumetric roughness parameter for the surface (R_v) and reported that for $R_v \leq 500\ nm$ drops are formed close to the top of the nano-structures and doesn't completely fill inside the cavities of nano-structures.

In this study, I am looking for an optimum first tier structure size in order to enhance the self-removal of drops during condensation and consequently improve heat transfer. Resistance energies toward the transition of a tail of a drop from within four squarely positioned first tier pillars to the top of the pillars are used in order to optimize surface roughness size. Viscous dissipation and work of adhesion are considered as dissipating consumptions which resist toward the transition of the tail of a drop. By minimizing the resistance energies I came up with an optimum size for the first tier of the hierarchical surface which could make the detachment of the tail of a drop from the base of the cavity and the entire drop from the surface easier.

In chapter 2 I am introducing superhydrophobic surfaces. The features of these surfaces when confronted with a drop are discussed. Chapter 3 explains about experiments on superhydrophobic surfaces using FEI Quanta ESEM. The surface coverage and mean droplet diameter of a superhydrophobic surface and a smooth hydrophobic surface during condensation are compared. Also the growth of a droplet in the cavities of the first tier pillars is captured using ESEM. This growth mechanism is used in the next chapter in order to come up with an approach to optimize the roughness size. Chapter 4 goes through details of my analysis which intends to find a way to optimize the size of first tier pillars in order to enhance droplet self-removal and consequently improve heat transfer and the results of my approach are discussed. Finally the results of my analysis are summarized in chapter 5.

CHAPTER 2

WATER REPELLENT SURFACES

Hydrophobic surfaces are referred to surfaces with low surface energy so that water drops sitting on them have contact angles greater than 90°. The term “superhydrophobicity“ is used for surfaces to show their high hydrophobicity. Superhydrophobic surfaces (SHS) show a very large contact angle when confronted with water. Sometimes contact angle 150° is introduced as an ad hoc criteria in order to distinguish between superhydrophobic and hydrophobic surfaces. Therefore surfaces with higher and lower contact angles than the aforementioned contact angle are called superhydrophobic and hydrophobic respectively despite the fact that this contact angle does not show a specific physical characteristic of the surface [17]. There are different examples of hydrophobic and superhydrophobic surfaces in the nature such as Shark skin, butterfly wings, water strider legs, etc [18]. Investigations have shown that the reason for these surfaces to show superhydrophobic characteristics is twofold: the asperities covering the surface and the wax or coating on the surface which makes it hydrophobic. Lotus leaf is one of the most famous examples [19]. The surface of the lotus leaf is covered with a wax as wells as two levels of roughness. The first level of roughness is micro-bumps which are covered with nano-hairs as a second level. The combination of the wax and the two levels of roughness give a lotus leaf a high level of hydrophobicity. Drops deposited on a lotus leaf are spherical and even a slight tilt of surface makes them roll off. Water repellency of these surfaces has prompted researcher to synthesize highly hydrophobic surfaces with the same characteristics by mimicking them. Different coatings as well as micro and nano-asperities have been

used to increase the roughness of the surface. The effects of the roughness shape and size on contact angle and contact angle hysteresis were abundantly investigated [20-28].

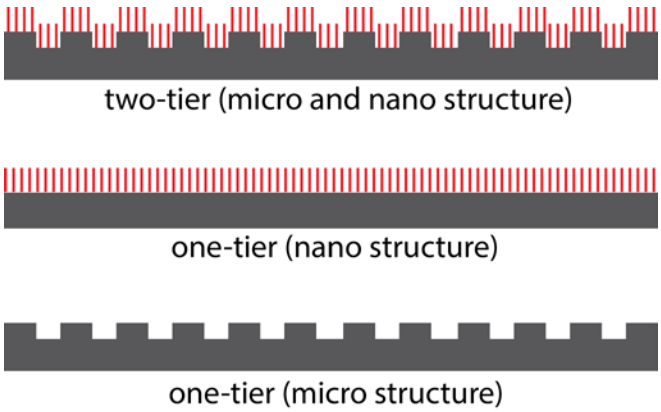

FIG. 2.1 One-tier and two-tier textured surfaces

1.1 Capillary Length

The dominant forces while dealing with micro/nano-scale are surface forces while gravity effect becomes negligible. Droplets in micro/nano-scale can stick to the surface in an upside down position disregarding the gravity effect. The surface tension between droplet and the surface are highly larger than gravity force which makes the drop to stay attached to the surface. Therefore the effect of gravity in a system beneath a particular length could be neglected. If hydrostatic pressure $\rho g \lambda_c$ for a liquid with density of ρ is comparable to the Laplace pressure $\frac{\sigma}{\lambda_c}$, a special length λ_c known as capillary length can be derived [29],

$$\rho g \lambda_c = \frac{\sigma}{\lambda_c} \implies \lambda_c = \sqrt{\frac{\sigma}{\rho g}} \tag{2.1}$$

For a size lower than capillary length the surface forces are dominant in a system. When a droplet with a size smaller than capillary length is deposited on a

surface, it forms a spherical cap. However droplets with larger sizes than capillary length is flatten as a result of gravity.

FIG. 2.2 Effect of capillary length on drop morphology

1.2 Young's Relation

A droplet in the space forms a sphere to reduce its surface energy. When the effect of the gravity is negligible due to the very small size of the droplet this phenomenon happens again. When this droplet sits on an ideal homogenous surface it forms a circular contact area which the periphery of this contact area is called the contact line where all the existing phases exist together. The liquid touches the solid at contact line with an angle which is known as contact angle. If the contact line of the liquid moves about dx then the change in the surface energy of the system could be written as [30],

$$dE = dx\cos\theta\,\sigma + dx\sigma_{sl} - dx\sigma_{sv} \tag{2.2}$$

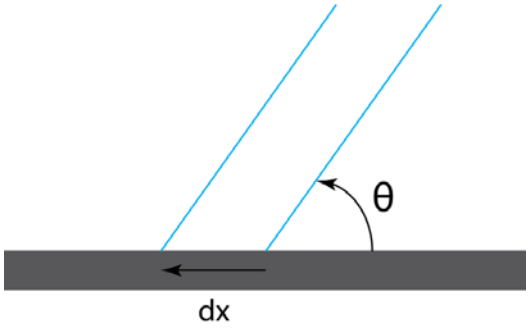

FIG. 2.3 Surface energy change as contact line moves dx on smooth surface

The droplet on the surface tends to have the lowest energy at equilibrium which yields the following equation known as Young's relation,

$$cos\,\theta = \frac{\sigma_{sv} - \sigma_{sl}}{\sigma} \tag{2.3}$$

FIG. 2.4 Young's contact angle and surface forces at contact line

The Young's relation can also be derived by applying force balance at the contact line of the droplet on the surface,

$$\sum F_{contact\ line} = \sigma_{sv} - \sigma_{sl} - \sigma \cos\theta = 0 \tag{2.4}$$

which clearly leads to equation 2.3.

1.3 Cassie-Baxter Model

On surfaces with high degree of roughness, drops tend to stay on top of roughness when they are deposited on the surface. Drops sitting on top of roughness with air pockets beneath them are called fakir drops [31]. When a drop sits on top of asperities of the surface the solid-liquid contact of the base of the drop is lowered. This reduction in solid-liquid contact which is replaced by liquid-air leads to an increase in drop contact angle because of 180° contact angle of water and air.

Contact angle of a drop in fakir state could be evaluated by taking an average between the contact angle of drop with solid and drop with air considering the portions of the drop which have contact with the substrate and with air,

$$\cos\theta^* = f\cos\theta_s + (1-f)\cos\theta_a \tag{2.5}$$

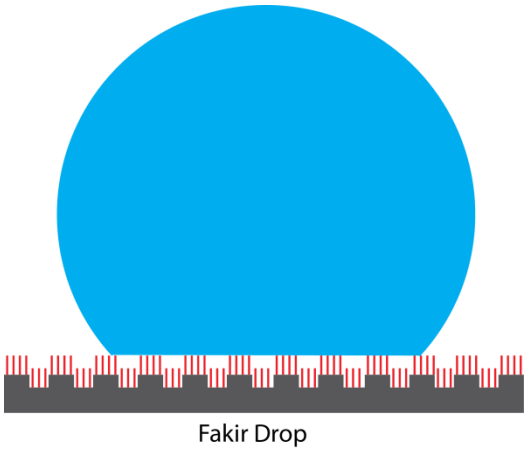

FIG. 2.5 Drop in Cassie-Baxter state; Sitting on top of surface roughness

where f is the solid fraction, θ_s is the contact angle of water and substrate and θ_a is the contact angle of water and air. The above equation was first proposed by Cassie [32, 33] predicting an enhancement of contact angle due to surface roughness. Fakir drops are also called Cassie drops or composite drops.

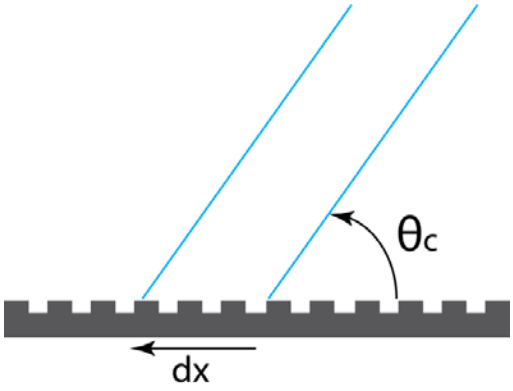

FIG. 2.6 Surface energy change as contact line moves dx on top of surface roughness

The same energy change analysis as smooth surface for an infinitesimal displacement of contact line could be carried out for droplets in Cassie state,

$$dE = f\sigma_{sl}dx - f\sigma_{sv}dx + \sigma dx\cos\theta_c + (1-f)\sigma dx \quad (2.6)$$

Minimizing the energy on the surface leads to the following equation for the contact angle of the drop in Cassie state,

$$\cos\theta_c = f(\cos\theta + 1) - 1 \quad (2.7)$$

The above equation is well known as Cassie-Baxter equation. It validates Cassie equation for contact angle of fakir drops (eq. 2.5). The contact angle of water with air is 180°, therefore $\cos\theta_a$ equals -1 and equation 2.5 transforms into the above equation.

1.4 Wenzel Model

Wenzel [34] mentioned that the hydrophobicity or hydrophilicity of the surface is amplified by the roughness of the surface. Based on Wenzel theory [35] the liquid follows all the asperities of the surface. Therefore the liquid-solid contact increases as the roughness of the surface increases. A roughness factor (r) was defined as the ratio of the actual surface to the geometric surface [35]. As the roughness factor gets larger, for $\theta > 90$ the hydrophobicity of hydrophobic materials increases and for $\theta < 90$ hydrophilicity of hydrophilic materials is intensified.

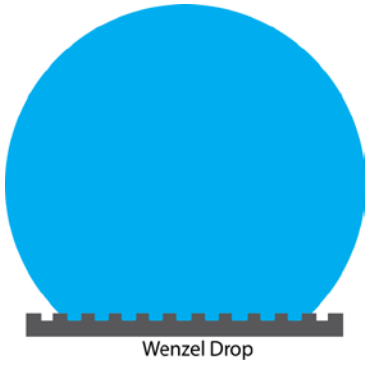

FIG. 2.7 Drop in Wenzel state; Filling the cavities of the roughness

When a droplet is deposited on a surface and it is in a so-called Wenzel state, it fills all the cavities of the roughness. To calculate the contact angle of the drop in Wenzel state, the change of energy of the drop while the contact line moves infinitesimally is derived,

$$dE = r\sigma_{sl}dx - r\sigma_{sv}dx + \sigma dx\cos\theta_w \tag{2.8}$$

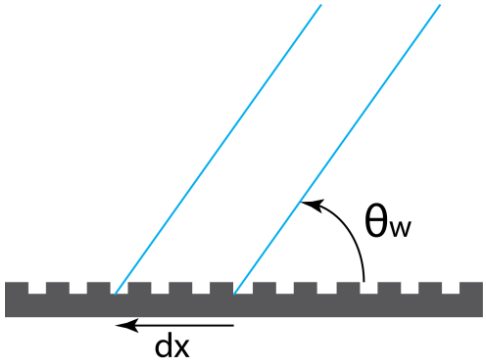

FIG. 2.8 Surface energy change as contact line moves dx in the cavities of surface roughness

By minimizing the energy on the surface, contact angle of a droplet in Wenzel state is calculated,

$$\cos\theta_w = r\cos\theta \tag{2.9}$$

1.5 Critical Contact Angle

The surface energy of a drop when it sits on a surface plays an important role in figuring out the state of the drop. Depending on the surface and its roughness morphology the drop deposited on the surface might have a lower surface energy in Wenzel state (Wenzel is the stable state and Cassie is the metastable state) or in Cassie state (Cassie is the stable state and Wenzel is the metastable state). When Wenzel state is the stable state of the surface, drops are more willing to fill the cavities

of the roughness. On the other hand when Cassie state is the stable state, drops are willing to sit on top of the roughness.

Based on my energy analysis on Wenzel and Cassie drops, by setting the contact angles of the drop on Cassie and Wenzel state equal, the point in which the stable state of the drop transitions from Wenzel to Cassie energetically can be found.

$$f(\cos\theta_c + 1) - 1 = r\cos\theta_c \tag{2.10}$$

$$\cos\theta_{cr} = -\frac{1-f}{r-f} \tag{2.11}$$

A drop on a surface with Young contact angle values greater than θ_{cr} has lower energy in composite or Cassie state which means drops deposited on a surface would stay on top of roughness whereas on a surface with θ values less than θ_c the Wenzel state is preferred and drops would fill the cavities of the roughness.

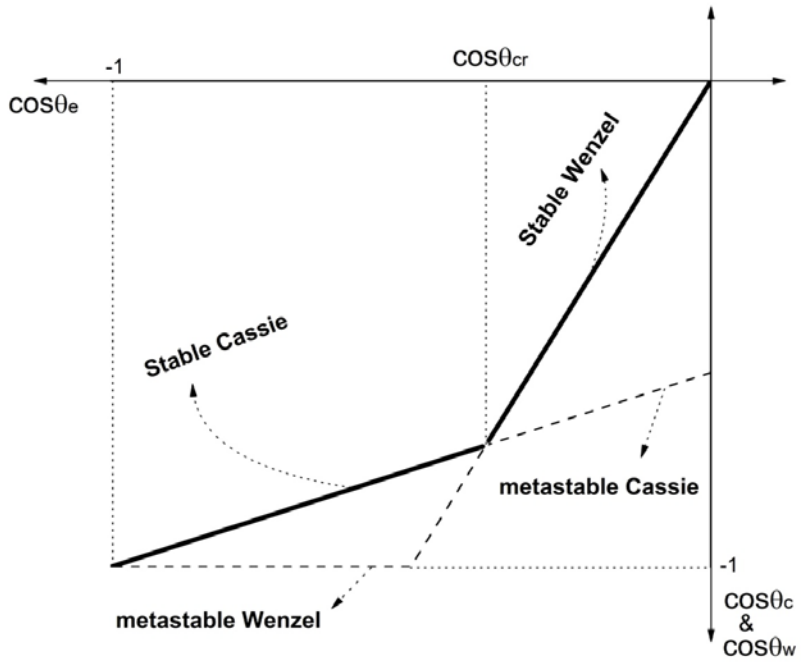

FIG. 2.9 Stable and metastable Cassie and Wenzel States

1.6 Contact Angle Hysteresis

A drop sitting on a surface resist toward movement by changing its advancing and receding contact angles. Advancing contact angle of a drop is the angle formed when the contact line is moving or is about to move towards the ambient medium and receding contact angle is the angle formed when the contact line is moving or is about to move towards liquid medium.

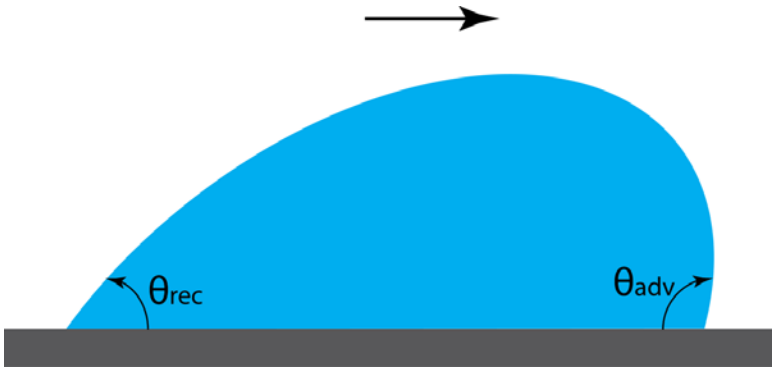

FIG. 2.10 Advancing and receding contact angles

The difference between advancing and receding contact angles are widely known as contact angle hyteresis [36]. When contact line faces an asperity on its way, pins over it which is known as pinning effect. As a result of the pinning effect the contact line of the drop diverges from its equilibrium (Young) contact angle until it moves over the pinning point. This process leads to stick and slip behavior of the dynamic contact line.

$$\Delta\theta = \theta_{adv} - \theta_{rec} \tag{2.12}$$

As it has been mentioned above heterogeneities of the surface lead to contact angle hysteresis. Therefore it is reasonable to expect a decrease in hysteresis as the drop-surface contact is lowered. For surfaces with roughness that can provide drops in Cassie state, due to less solid-liquid interface contact angle hysteresis decreases.

Consequently drops on these surfaces are more easily removed from the surface. For drops in Wenzel state as a result of increase in solid-liquid interface contact angle hysteresis is intensified which leads to sticky drops.

1.7 Work of Adhesion

When a liquid touches a solid surface a new solid-liquid interface is formed. During this process both solid-vapor and liquid-vapor interfaces are replaced with solid-liquid interface. This change of interface results in a change in surface energy of the system. In the case of a liquid being detached from a surface the reverse process happens. First there is a liquid-solid contact which is replaced with solid-vapor and liquid-vapor interfaces after detachment. The change of energy during the process of detachment is well known as work of adhesion [29],

$$W_{adh} = \sigma + \sigma_{sv} - \sigma_{sl} = \sigma(1 + \cos\theta) \tag{2.13}$$

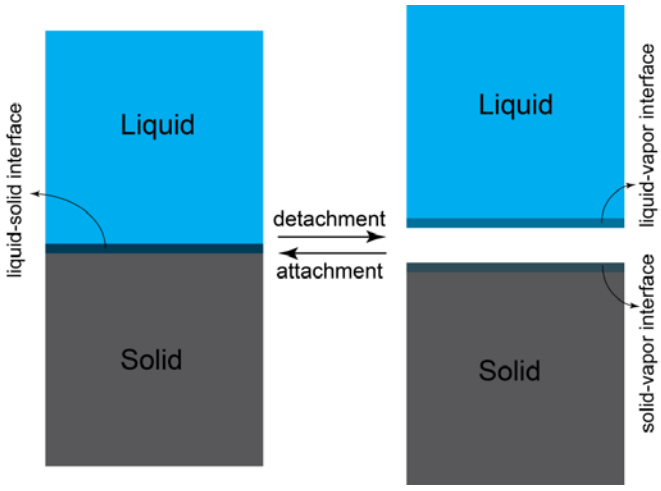

FIG. 2.11 Interface formation during attachment and detachment of liquid and solid medium

CHAPTER 3

EXPERIMENTAL PROCEDURE

1.8 Surface Structure

Squarely positioned micro-pillars were formed on a 2 cm × 2 cm silicon surface using deep reactive ion etching (DRIE). Subsequently a thin layer of nickel was coated on the etched silicon substrate to work as a catalyst. Carbon nano-tubes (CNT) were grown afterwards by plasma enhanced chemical vapor deposition (PECVD). To make the surface hydrophobic a thin layer of fluoropolymer (FluoroPel™ PFC1601V, Cytonix Corporation) was coated on the surface [14]. A scanning electron microscopy (SEM) was used in order to measure the micro/nano-structure sizes. The micro-pillars on the surface were 5.5 μm in width, 4 μm in height with a pitch spacing of 8.5 μm. The nano-tubes were approximately 160 nm in diameter, 400 nm in height. The nano-tube solid fraction was around 0.2 calculated using SEM top view images of nano-tubes.

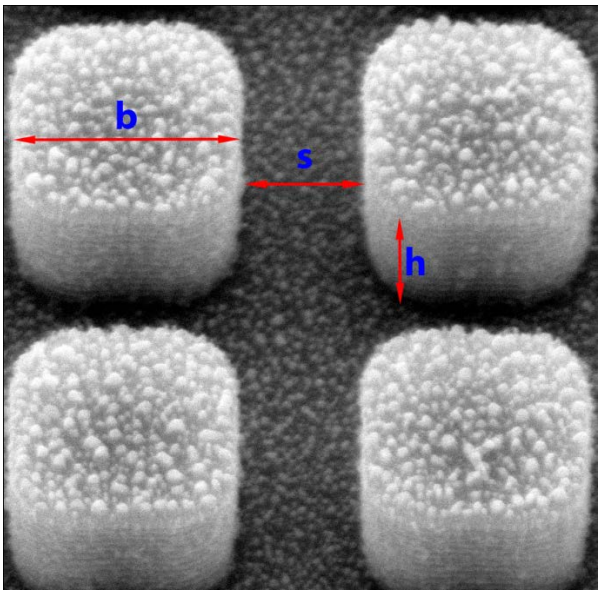

FIG. 3.1 ESEM image of two-tier surface; four squarely positioned micro-pillars

$$b = 5.5\ \mu m$$

$$s = 3\ \mu m \tag{3.1}$$

$$h = 4\ \mu m$$

The solid fraction of micro-scale on the surface could be calculated as follows

$$f_m = \frac{b^2}{(b+s)^2} = 0.42 \tag{3.2}$$

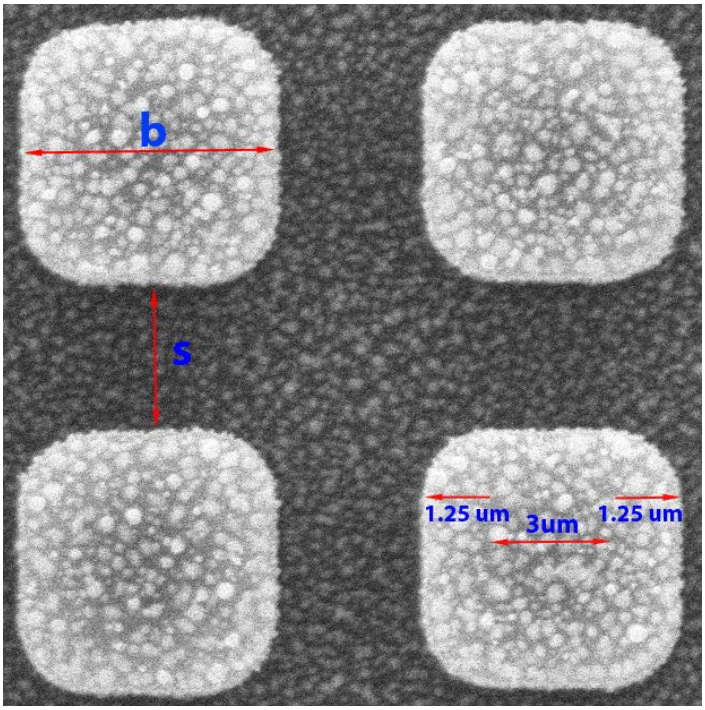

FIG. 3.2 ESEM image of two-tier surface; top view of four squarely positioned micro-pillars

A more accurate look at the micro-pillars on the surface shows that the corners of the pillars are rounded as it is shown in figure 3.2. To consider that in the calculation of solid fraction, r_p was defined which denotes the radius of corner of the pillars and in the case of my surface is 1.25 μm. Therefore the solid fraction of micro-pillars could be rewritten as

$$f_m = \frac{b^2 - 4({r_p}^2 - \frac{\pi}{4}{r_p}^2)}{(b+s)^2} = \frac{b^2 - (4-\pi){r_p}^2}{(b+s)^2} = 0.4 \quad (3.3)$$

The fluoropolymer that I have used on the surface has a contact angle of 115°. The contact angle of a drop on top of the nano-structure and hierarchical structure could be quantified using Cassie-Baxter theory,

$$\cos\theta_n = f_n(\cos\theta + 1) - 1 \implies \theta_n = 152° \quad (3.4)$$

$$\cos\theta_{mn} = f_m f_n(\cos\theta + 1) - 1 \implies \theta_{mn} = 162° \quad (3.5)$$

where θ is Young's contact angle on smooth surface, θ_n is apparent contact angle of drops on nano-tubes and θ_{mn} is apparent angle of drops on hierarchical surface.

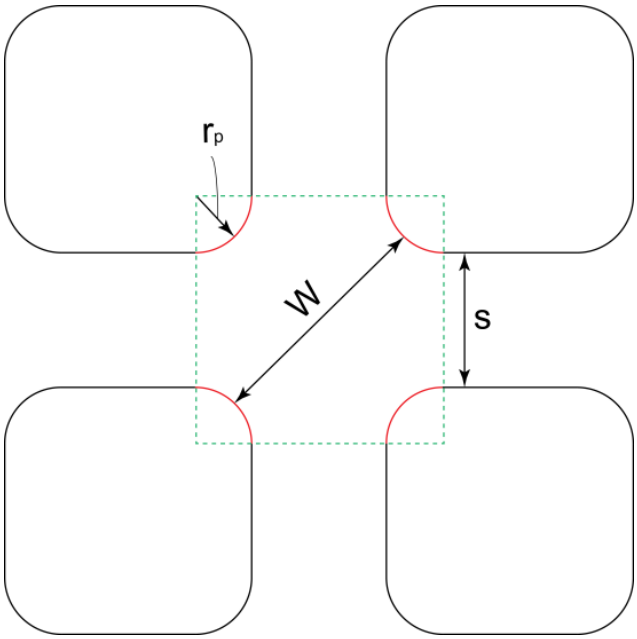

FIG. 3.3 Distance between diagonal pillars (W)

There is another parameter which will be used later in my analysis which is the diagonal distance between the corners of the pillars (W) as it is shown in figure 3.3. The value of W could be calculated based on the roughness sizes as follows,

$$W = \sqrt{2(s + 2r_p)^2} - 2r_p \tag{3.6}$$

In the case of my surface the value of W is

$$W = \sqrt{2(3 + 2 \times 1.25)^2} - 2 \times 1.25 = 5.278 \tag{3.7}$$

FIG. 3.4 FEI Quanta 250 environmental scanning electron microscope

1.9 Condensation Experiments

The condensation experiment was carried out on two-tier and smooth surfaces hydrophobicized by fluoropolymer coating (FluoroPel^{TM} PFC1601V) using ESEM (FEI Quanta 250) to investigate the characteristics of these surfaces during condensation. The samples were cooled down inside ESEM using a Peltier cooler. When a single drop is located on a smooth surface the contact angle of the drop is different than a drop on

two-tier surface. In the case of my two-tier surface which has micro pillars covered with nano-tubes to form the double scale structure, the droplet stands on top of the hierarchical structure which is known as Cassie state. Cassie theory states that drops on very rough surfaces stay on top of roughness with air pockets beneath the drop which could increase contact angle and decrease contact angle hysteresis in comparison with smooth surface. However condensation is a dynamic process and it is important to check out and see if the characteristics of two-tier surfaces such as low hysteresis still hold during condensation.

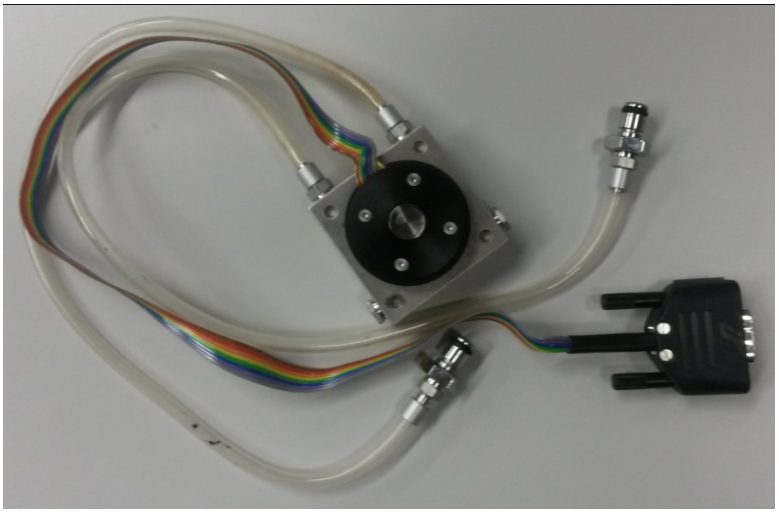

FIG. 3.5 Peltier cooler

Figure 3.6 shows the condensation of water vapor on a smooth surface monitored by ESEM. As it is shown the nucleates on the smooth surface start to grow without any interaction with adjacent drops until a specific size which drops touch each other and subsequently coalescence starts to affect the growth. Drops merge together and form larger drops and consequently cover most of the surface during condensation on a smooth surface.

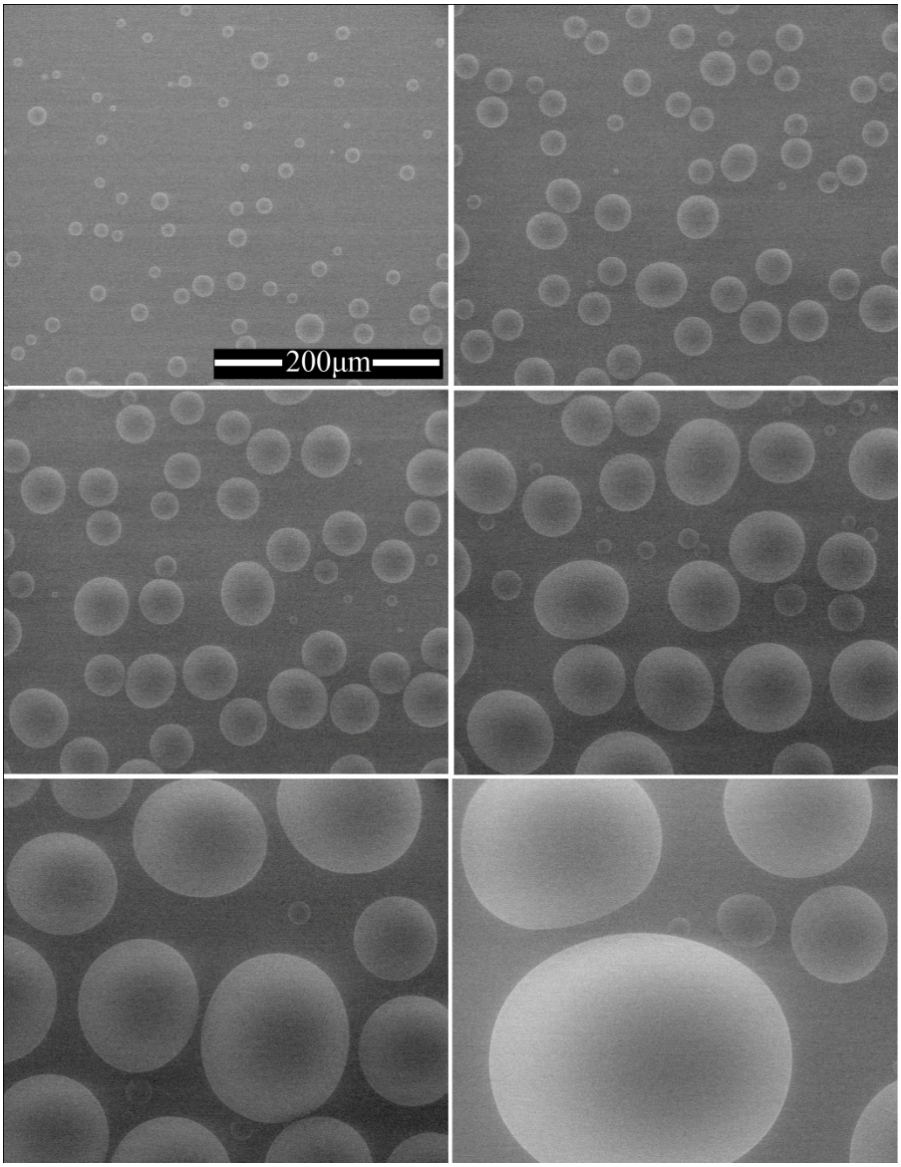

FIG. 3.6 Condensation on smooth surface captured by ESEM (12.5 kV, 4.8 Torr)

Condensation on two-tier surface is indicated in figure 3.7. More nucleation sites could be seen at the beginning of condensation which could be attributed to the asperities of the surface. At the beginning of condensation nucleates grow until they reach the adjacent droplets and then coalescence affects the growth of droplets. Unlike smooth surface drops of large size couldn't be found on two-tier surface. On my

hierarchical surface the largest droplet during condensation was around 100 μm. To illustrate the reason behind different behaviors of smooth and two-tier surfaces during condensation, I have checked drops at specific points on both surfaces before and after coalescence to see the difference between these two surfaces.

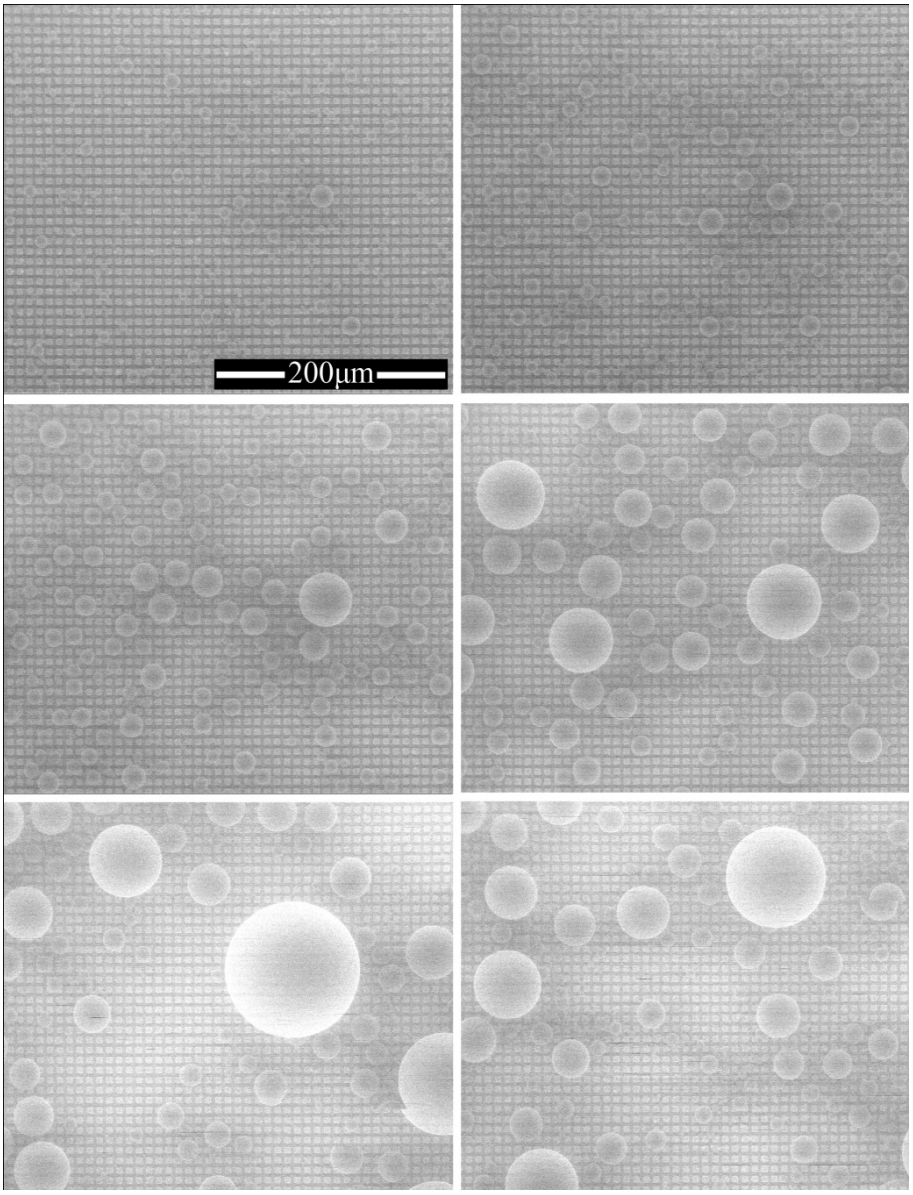

FIG. 3.7 Condensation on two-tier surface captured by ESEM (12.5 kV, 4.8 Torr)

Figure 3.8 shows two points on the smooth surface before and after coalescence. The droplets are attached to the surface before and after coalescence at both points. The droplets merge together to form a larger droplet and while the center of gravity of the drops change due to coalescence, the drops are still attached to the surface with negligible change in a position.

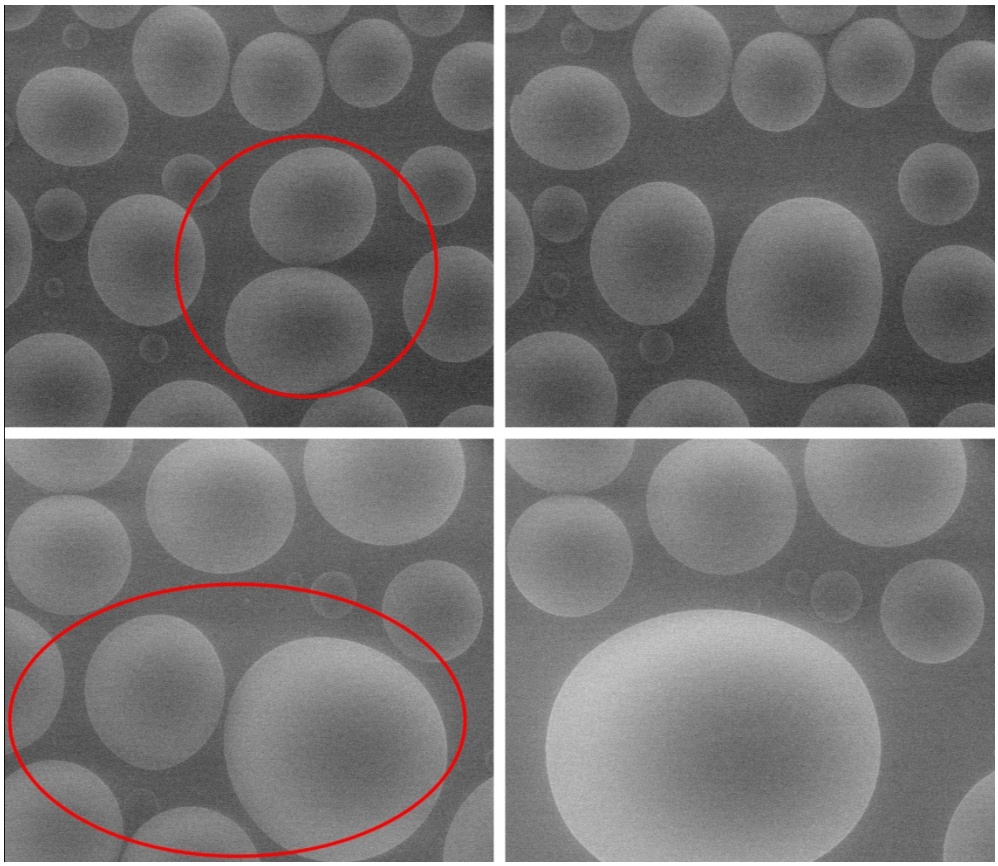

FIG. 3.8 Coalescence of droplets on smooth surface

The coalescence of droplets on two-tier surface is illustrated at four points in figure 3.9. The coalescence process on superhydrophobic two-tier surface was observed to be more mobile than smooth surface. Interestingly the droplets leave the surface after coalescence happens which is the reason why drops of larger than specific size couldn't be found on two-tier surface during condensation. This self cleaning ability

of two-tier surface which is ascribed to the coalescence induced jumping [7] of droplets is an outstanding feature of these surfaces which could be exploited to increase bare surface during condensation and lower the resistance energy towards formation of new nucleation.

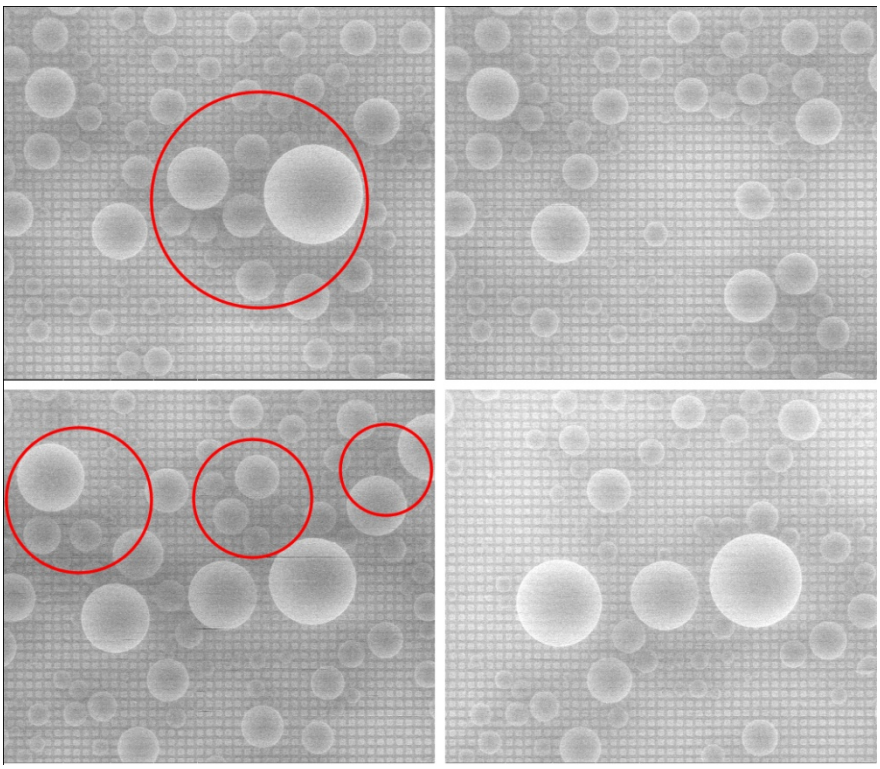

FIG. 3.9 Coalescence of droplets on two-tier surface

In order to investigate the effect of self cleaning during condensation, the average size of drops during condensation on both smooth and two-tier surface was calculated and plotted in figure 3.10. On the smooth surface the average diameter of the drops on the surface increases during condensation. Drops coalesce with each other and make larger drops and because of the adherence of them to the surface the average droplet diameter is increasing. On the contrary the average drop diameter on

two-tier surface rises at the beginning of condensation but after a while it levels out at average amount of around 15 μm as it can be seen on figure 3.10. This could be explained by a self cleaning ability of two-tier superhydrophobic surfaces during condensation. Drops start to coalesce all over the surface after a while and consequently leaving the surface as a result of coalescence-induced jumping which causes the average drop diameter to level out on two-tier surface.

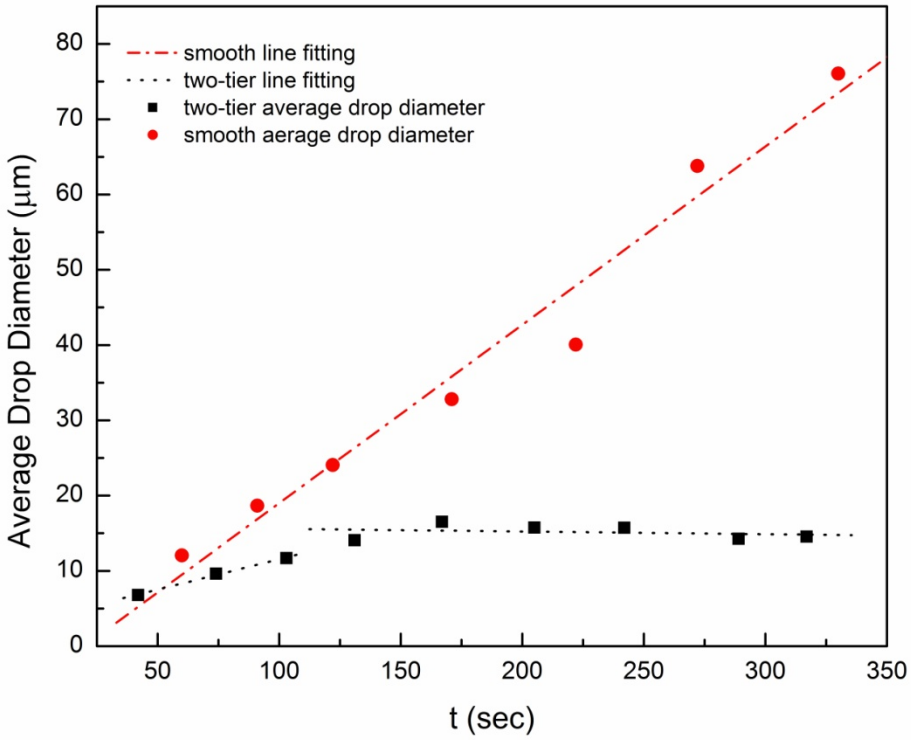

FIG. 3.10 Average droplet diameter variation vs time for smooth and two-tier surface

The surface coverage of droplets on both smooth and two-tier surfaces is plotted versus time in figure 3.11. Surface coverage on both surfaces (smooth and two-tier structure) flattens out after a while. For smooth hydrophobic surface the surface

coverage levels out at 0.58 while the superhydrophobic surface coverage flattens out at around 0.28 which is almost half of the smooth surface coverage. Increase of bare surface on two-tier structure could be interpreted as less resistance towards new condensate formation which can possibly increase the rate of condensation and subsequently increase heat transfer.

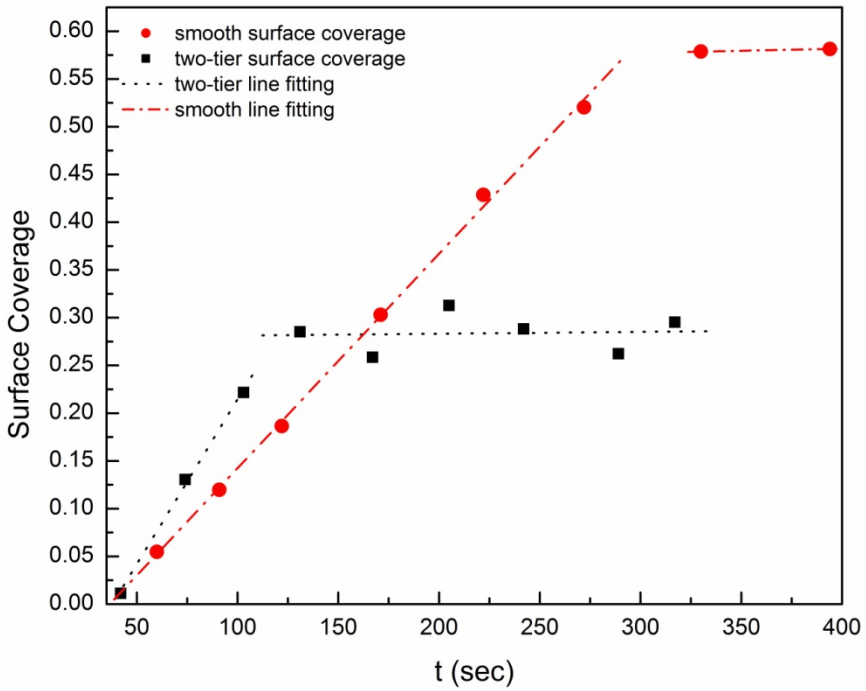

FIG. 3.11 Surface coverage variation versus time for smooth and two-tier surface

It is difficult to prevent nucleates to form in the cavities of micro and nano-pillars due to the critical nucleation radius of water which is around tens of nano-meter. Therefore nucleation starts to grow among roughness cavities of the two-tier surface. As a result of lower surface energy micro-droplets in the cavity are mostly formed at the lower corner of the micro-pillars of the surface as it is shown in figure 3.12.

Subsequently Laplace pressure works as a driving force to propel the droplet between four pillars to maintain a lower surface energy. The lateral movement of the droplet continues until it touches the adjacent micro-pillars and then it starts to grow upward and reaches the top of the micro-pillars and spreads over them. This process is used in my analysis in order to figure out a way to optimize the first tier of the surface.

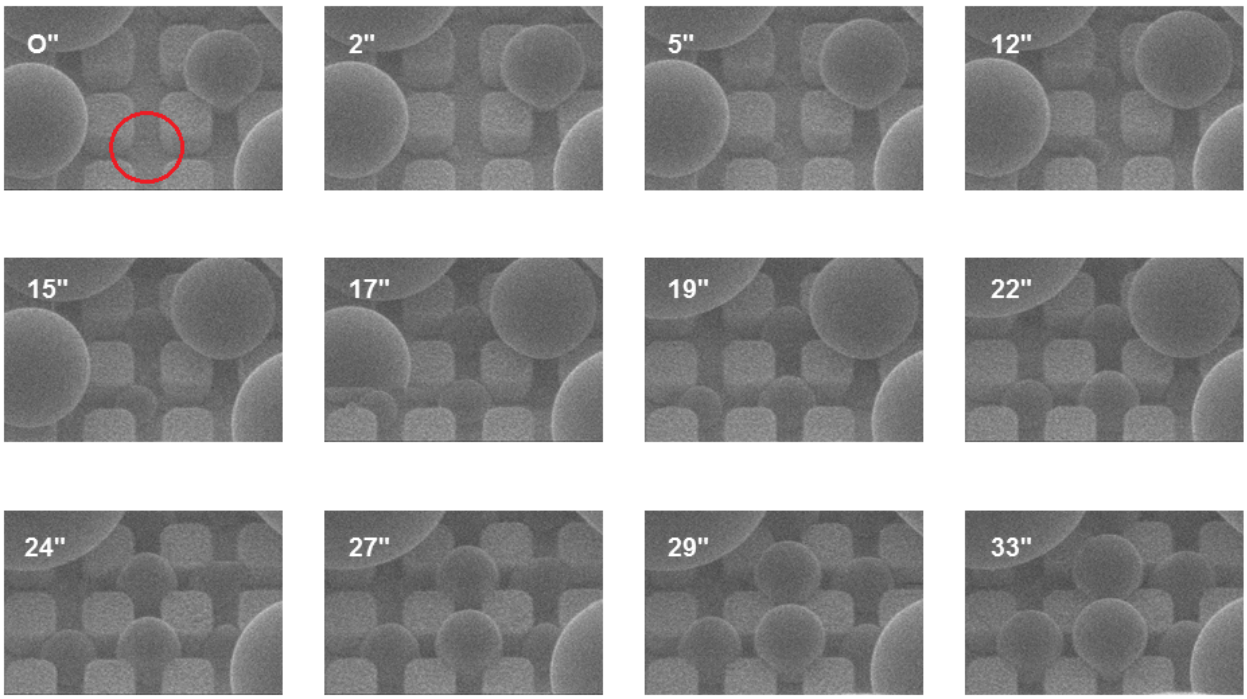

FIG. 3.12 Growth of droplet in the cavity of first tier of the hierarchical superhydrophobic surface

CHAPTER 4

RESULTS AND ANALYSIS

1.10 Overview of the Problem

Condensation of water vapor on hydrophobic substrates which resist wetting of their surfaces results in dropwise condensation. These surfaces enhance heat transfer significantly in comparison to filmwise condensation. However on a smooth hydrophobic surface there needs to be a driving force to detach drops from the hydrophobic surface. Typically weight of drops is being used as a driving force which makes surfaces to be able to shed drops with diameters larger than capillary length. One of the intriguing characteristics of superhydrophobic surfaces is coalescence-induced jumping which is referred to jump of droplets after merging with each other. This phenomenon leads to removing drops from the surface which happens even for droplets extremely smaller than capillary length. This jumping event has nothing to do with the orientation of the surface which means even for horizontal surfaces (no gravity) owing to coalescence-induced jumping, dropwise condensation could be observed by repeatedly providing bare surface for continuous condensation.

In my analysis I am willing to optimize the size of the micro-structure to facilitate coalescence-induced droplet removal and consequently improve heat transfer. I need to simplify the formation of nucleate, growth of droplet and droplet coalescence in order to come up with a theoretical analysis to optimize the structure. It is more desired to have drops in Cassie state than in the Wenzel state while seeking droplet self-removal due to lower pinning of Cassie droplets to the surface. However it is difficult to tailor a structured surface resisting nucleation in the cavities especially micro-cavities of the

surface due to the small critical radius of water (tens of nano-meter). Therefore most of the droplets are formed within cavities of the surface which eventually forms a droplet in Wenzel state or partly Wenzel state.

It is imperative to have structures which resist lateral growth of droplets formed in the cavities. The more a droplet grows laterally within micro-pillars, the more pinning to the surface and the more contact with the base is generated and consequently less chance to have Cassie drops or less chance to remove a drop from the surface. If the surface is capable of resisting the lateral growth of the droplet in the cavity, drops would grow upwards and then sit on top of micro-pillars and the rest of the growth occurs on top of asperities of the surface, i.e., drops grow while the leading contact line is in Cassie state. Therefore there is always a tail of droplet within the cavity which needs to be removed in order to have an entire Cassie state.

Different external actuating methods (inducers) have been exploited in order to actuate the droplet or part of it such as mechanical vibration [37], electrical switching [38], electrical field [39], etc. However the only intrinsic driving power which could possibly change the state of drops from Wenzel state to Cassie state or remove drops from the surface during condensation is the energy released due to coalescence. Coalescence and coalescence-induced jumping widely happens on superhydrophobic surface during condensation. Therefore in order to exploit this released energy, dissipating consumptions during the Wenzel to Cassie transition or removal from the surface needs to be minimized.

In my analysis I am focusing on the tail of droplet sticking within four micro-pillars and disregard the mass the drop above the pillars. I am not concerned with released

energy as a result of coalescence which works as a driving force but the energy which needs to be overcome to transition the tail to the top portion of the drop (resistance energy). The solid fraction of the surface is maintained at constant value while the effect of changing the size of pillars on resistance energies of the cavity is investigated. fixing the solid fraction of the surface indicates that while the size of pillars are changing, droplets of the same size sitting on these pillars have the same surface energy regarding the top portion of the drop but they might have different energy within the cavities of the surface. I specifically investigate adhesion energy of the condensate base and viscous dissipation of condensate tail inside a cell to minimize the dissipating sources resisting the transition of the tail of droplet in the cavity.

1.11 Required Energy to Detach a Droplet in a Cavity

A droplet grows within four micro-pillars and places itself among them in a way that touches the corners of surrounding pillars. The diameter of the drop between the micro-pillars can be assumed to be the same as W as shown in figure 4.1. The base diameter of the droplet in the cavity could be calculated using the contact angle of the drop on nano-structures and the radius of the droplet as follows,

$$W = 2R_1 \tag{4.1}$$

$$r = R_1 \sin\theta_n \tag{4.2}$$

Assuming that the droplet sits on top of the nano-tubes in the cavity of micro-pillars, the contact of drop with the solid surface in cavity would be,

$$A_{adh} = f_n \pi {R_1}^2 \sin{\theta_n}^2 \tag{4.3}$$

where f_n is the solid fraction of CNT nano-structures which in my sample is 20%. As it was mentioned before during the detachment of the droplet from the surface the liquid-vapor and solid-vapor interfaces are formed and replaced with liquid-solid interface. Energy change during the detachment of the base could be found using the work of adhesion of the surface.

$$W_{adh} = \sigma(1 + \cos\theta) \tag{4.4}$$

So the energy required to detach a droplet from the base is,

$$E_{adh} = W_{adh} \times A_{adh} = \sigma(1 + \cos\theta) \times f_n \pi {R_1}^2 \sin {\theta_n}^2 \tag{4.5}$$

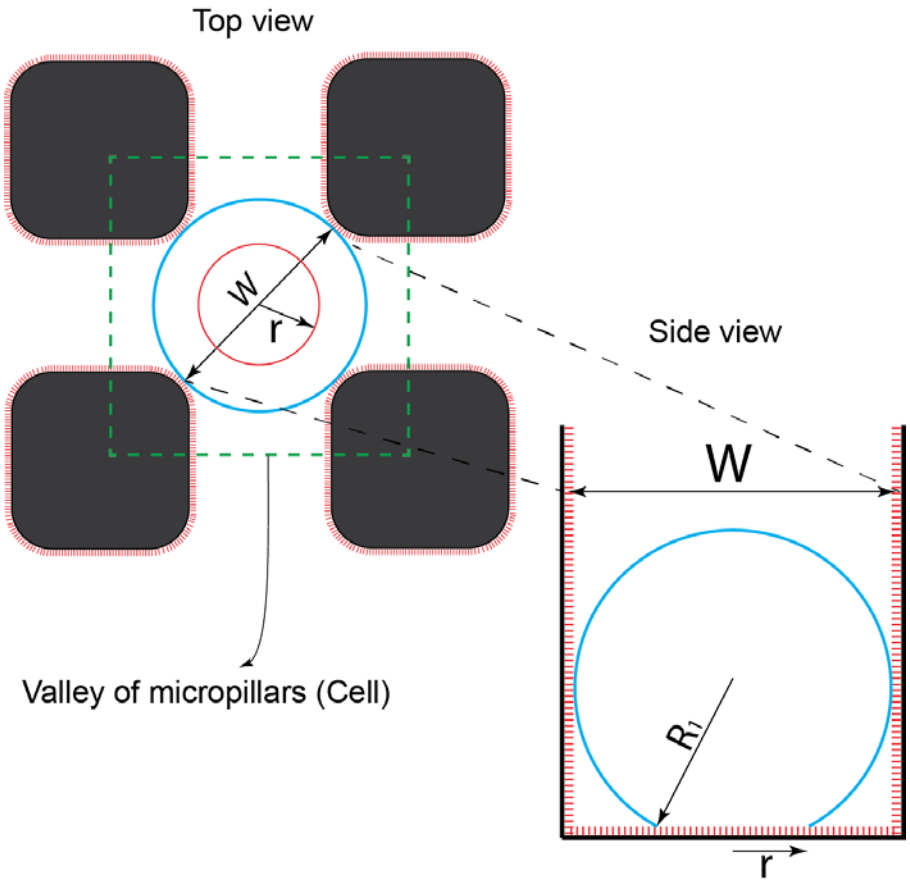

FIG. 4.1 Droplet growth between four squarely positioned first tier pillars

1.12 Viscous Dissipation

During the process of expulsion of the tail of drop from the cavities of micro-pillars, viscous dissipation plays a significant role in wasting the driving energy which is expected to expel the tail out of the cavity, i.e., transition of the tail from Wenzel state to Cassie state. It is impossible to precisely calculate viscous dissipation during expulsion due to intricacy of the whole process. However it is possible to use the scaling law to estimate this value.

The energy lost as a result of viscous dipssipation during a finite time to deform a volume of liquid can be estimated as [40],

$$E_{vis} = \int_0^{\tau} \int_{\Omega} \Phi d\Omega dt \approx \Phi \Omega \tau \tag{4.6}$$

where Ω is the volume of the liquid in the cavity and τ is the period of viscous dissipation and Φ is the dissipation function. The process of expulsion starts as a tail of liquid entrapped among four micro-pillars moves upward as a result of coalescence of top portions of drops on top of micro-pillars. To simplify the whole process the tail of liquid is considered to be circular so that I can use viscous dissipation function in cylindrical coordinate as follows

$$\begin{aligned} \Phi = 2\mu \left\{ \left(\frac{\partial u_R}{\partial R}\right)^2 + \left[\frac{1}{R}\left(\frac{\partial u_\theta}{\partial \theta} + u_R\right)\right]^2 + \left(\frac{\partial u_z}{\partial z}\right)^2 \right\} \\ + \mu \left\{ \left(\frac{\partial u_\theta}{\partial z} + \frac{1}{R}\frac{\partial u_z}{\partial \theta}\right)^2 + \left(\frac{\partial u_z}{\partial R} + \frac{\partial u_R}{\partial z}\right)^2 \right. \\ \left. + \left[\frac{1}{R}\frac{\partial u_R}{\partial \theta} + R\frac{\partial}{\partial R}\left(\frac{u_\theta}{R}\right)\right]^2 \right\} \end{aligned} \tag{4.7}$$

Considering the expulsion process as a one dimensional process in z direction (vertical), above expression could be simplified as,

$$\phi = \mu\left(\frac{\partial u_z}{\partial R}\right)^2 \tag{4.8}$$

Using scaling law to figure out the viscous dissipation function,

$$\Phi = \mu(\frac{\partial u}{\partial r})^2 \approx \mu\left(\frac{U/2}{W/2}\right)^2 \approx \mu\left(\frac{U}{W}\right)^2 \tag{4.9}$$

where r is replaced with half of W which is the diagonal distance between the corners of micro-pillars and u is replaced with the average velocity of the tail which is supposed to be zero at the beginning of the expulsion and U at the end.

To find out the value of U, it is assumed that expulsion happens as a result of pressure difference between the bottom and top of tail after detachment from the base. The value of the pressure at the bottom of the tail is estimated by assuming that a bottom side of the tail is spherical which is reasonable due to the fact that it is extremely smaller than capillary length of water. So the curvature of the bottom can be evaluated as [29],

$$r \approx \frac{W}{2\cos(\pi - \theta_n)} \tag{4.10}$$

Considering the value of the pressure at the top of the tail or over micro-pillars as zero due to the relatively larger radius of liquid on top, the pressure difference between the top and bottom side of the tail can be estimated as,

$$\Delta P = \frac{2\sigma}{r} \approx \frac{4\sigma}{W}\cos(\pi - \theta_n) \tag{4.11}$$

Therefore the force acting on the whole tail during expulsion can be estimated as,

$$F \approx \frac{4\sigma}{W}\cos(\pi - \theta_n) \times \frac{\pi W^2}{4} \approx -\pi\sigma W\cos\theta_n \tag{4.12}$$

Supposing the whole process of expulsion happens within time τ, by momentum law,

$$F \times \tau = m \times U \Longrightarrow U = \frac{F \times \tau}{m} \tag{4.13}$$

Now the only unknown variable to calculate viscous dissipation is the period of viscous dissipation τ. The average velocity can be assumed to be $U/2$ and considering the fact that mass center of the liquid in the cavity moves about $h/2$ which h is the height of micro-pillars the time needed for this movement is approximately scaled as

$$\tau \approx \frac{h/2}{U/2} = \frac{h}{U} \tag{4.14}$$

The mass of the tail in the cavity could be calculated roughly by the following relation,

$$m \approx rho \times \frac{\pi W^2}{4} h \tag{4.15}$$

Replacing above relations for F and τ and m into equation 4.12, a relation for U could be achieved as,

$$U = \frac{F \times t}{m} \Longrightarrow U^2 = \frac{F \times h}{m} \Longrightarrow U^2 \approx \frac{-\pi\sigma W \cos\theta_n}{rho \times \frac{\pi W^2}{4} h} \times h \approx \frac{-4\sigma \cos\theta_n}{rho \times W} \tag{4.16}$$

Therefore the expression for viscous dissipation is scaled as,

$$E_{vis} \approx \Phi\Omega\tau \approx \mu \left(\frac{U}{W}\right)^2 \times \frac{\pi W^2}{4} h \times \frac{h}{U} \approx \frac{1}{4}\pi\mu h^2 U \tag{4.17}$$

$$E_{vis} \approx \frac{1}{2}\pi\mu h^2 \sqrt{\frac{-\sigma \cos\theta_n}{rho \times W}} \tag{4.18}$$

1.13 Resistance Energy

To find an appropriate size for the first tier of the surface (micro-pillars), the resistance energy of the cavity is calculated as a function of the size of pillars (b). The resistance energy could be written as a summation of adhesion energy and viscous dissipation,

$$E_{resist} = E_{adh} + E_{vis} \tag{4.19}$$

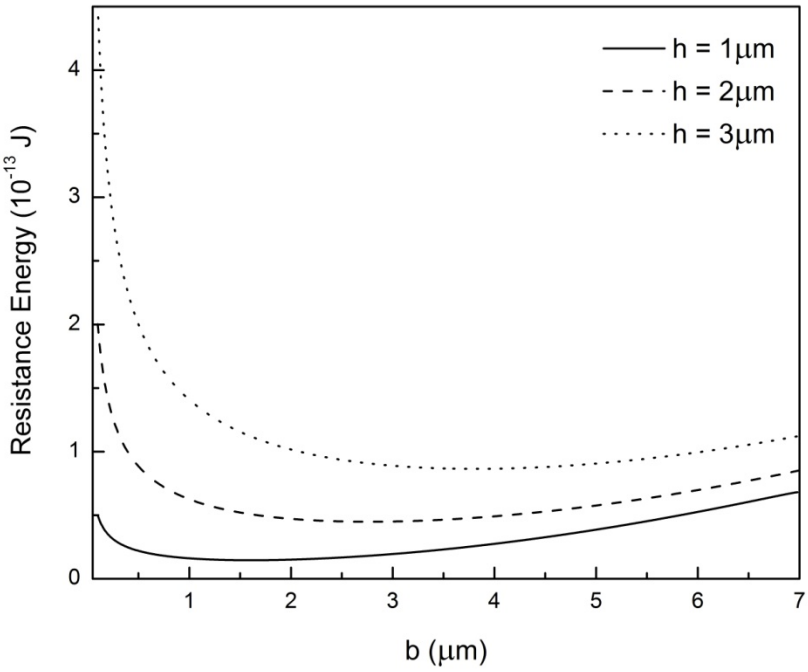

FIG. 4.2 Resistance energy of a single cell versus size of first tier pillars ($f = 0.08$)

As it was mentioned before the value of solid fraction is constant while the size of pillars is changed. Figure 4.2 demonstrates the variation of resistance energy versus pillar size. It could be seen that there is an optimum pillar size which minimizes the resistance towards transition of a single tail of liquid entrapped among four pillars. In my analysis as h decreases the optimum value of micro-pillars decreases so that for a pillar

height of 1 μm the optimum pillar width (b) is around 1 μm. For b values greater than the optimum size the dominant resistance towards transition is adhesion energy of the base and as pillar width gets smaller than the optimum size the dissipation function plays a prominent role in dissipating the driving energy or resisting towards transition of the tail.

It has been mentioned that I am working on two-tier surface with nano-structure as a second tier while the first tier is being modified to lower the resistance energy. So far I have optimized the size of micro-pillars based on the value of adhesion energy of the base and viscous dissipation of a single tail of drop. In figure 4.2, the height of pillars was kept constant while varying the width of micro-pillars. When the value of solid fraction (f) is fixed and the width of micro-pillars is changed, the micro-structures are simply being scaled up and down. However in the case of the above minimization the calculation is subject to a constraint on the value of h which is fixed for each curve. In the following calculation of resistance energy towards the transition of the tail of drop, the value of solid fraction is held constant. Also the height of pillars is scaled up and down together with the width of pillars and the behavior of resistance energy is studied. As shown in figure 4.3 the resistance energy is plotted for three different h to b ratios. As the width of micro-pillars decreases the energy which needs to be overcome to transition the tail of droplet falls down. It could be observed that by varying h along with b (fixing the ratio of h/b) the optimum value seen in the previous figure disappears. Figure 4.3 demonstrates the necessity of smaller sizes for the first tier of hierarchical surfaces [41, 42]. As the first tier moves to nano-scale the resistance energy is lowered. Therefore it is more appropriate to have double-tier structures both in nano-scale than having one of the tiers in micro-scale.

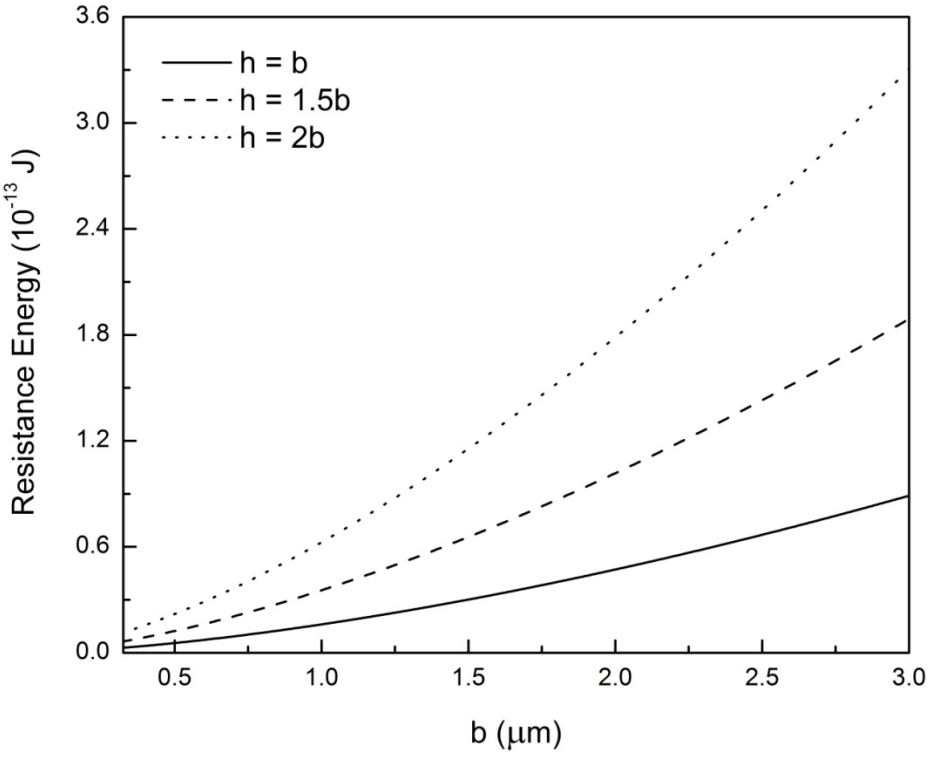

FIG. 4.3 Resistance energy of a single cell versus size of first tier pillars for different h to b ratios ($f = 0.08$)

I have analyzed the resistance energy towards the transition of a single tail in a single cell of the textured surface. It is more desirable to know the resistance energy of the entire surface in order to compare different surfaces. If the number of nucleation sites is controlled so that it is the same while changing the surface roughness, then the same trend as seen in figure 4.3 for a single cell is obtained for an entire surface. Therefore by controlling the number of nucleation density and keeping it constant as the size of pillars is changing, the resistance energy of the entire surface decreases as the size of pillars is decreasing. With the lack of an exact relation and experimental studies on the effect of surface roughness on nucleation density, it is difficult to figure out a way

to predict an exact value of nucleation density of the surface while the size of roughness is changing. However the importance of controlling the nucleation density in my analysis could be evidently shown by selecting different hypothetical curves demonstrating the effect of surface roughness on nucleation density.

In order to calculate the resistance energy of the entire surface during condensation, nucleation density of the surface for different roughness sizes should be known. There are not many papers investigating the effect of surface roughness and the size of it on nucleation density during condensation. Chen et al. [12] calculated the drop number density on four surfaces with different roughness. They mentioned that as the density of the micro-pillars increased the number of active nucleation sites raised. Lo et al. [43] also mentioned an increase in nucleation sites as the micro-grooves density was raised. It could be concluded that as the size of micro-pillars decreases on the surface while fixing solid fraction of the surface, the nucleation sites are increasing.

In order to have continuous dropwise condensation the coalescence should not hinder the process of micro-droplet growth among four mico-pillars, otherwise the surface would flood and dropwise condensation could not continue. To satisfy this criterion the spacing between the nucleation sites (L) should be at least 2 times the roughness spacing (l) which could be shown as $\frac{L}{l} > 2$ [44]. The spacing between nucleation sites could be shown as $L = \frac{1}{\sqrt{N_s}}$ where N_s denotes the number of nucleation sites. Using this relation the above criterion could be rewritten as

$$N_{s_{critical}} \leq \left(\frac{1}{2l}\right)^2 \tag{4.20}$$

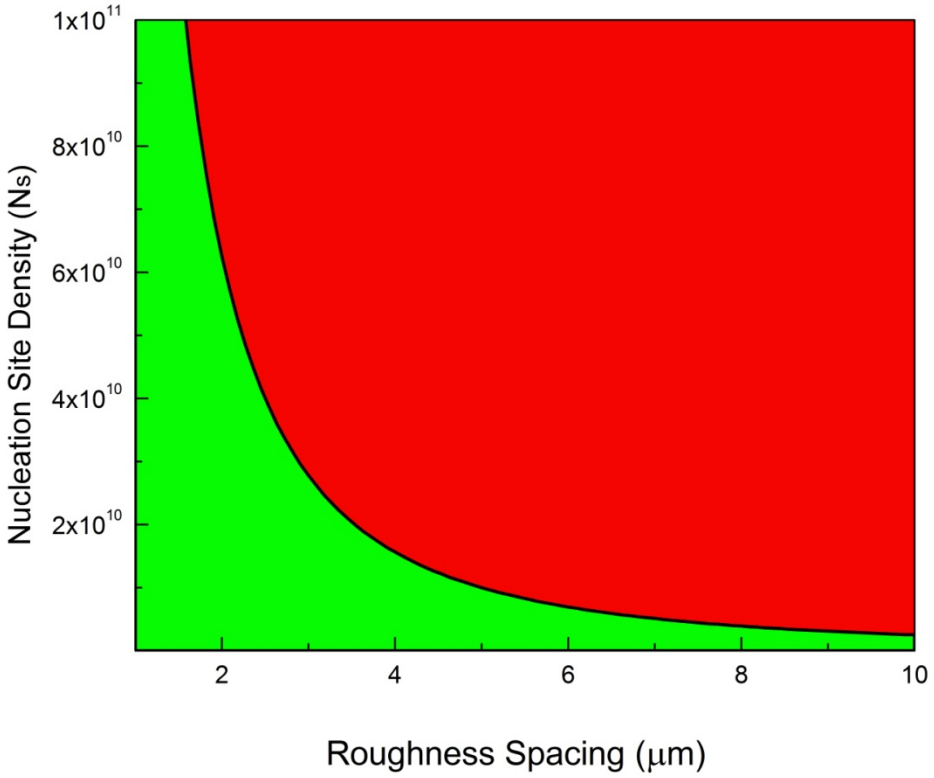

FIG. 4.4 Critical nucleation site density (N_s) for different roughness (l) spacing

Figure 4.4 shows the critical number of nucleation sites versus roughness spacing (Equation 4.19). As it is shown the area beneath the curve (green area) represents the nucleation sites which satisfy dropwise condensation criterion mentioned above. For N_s values over the curve (red area) dropwise condensation could not be observed due to coalescences within roughness of the surface which lead to flooding the surface.

Using the critical nucleation points regarding the surface ($N_{s_0} = \left(\frac{1}{2l_0}\right)^2$ where $l_0 = 8.5\ \mu m$) as a starting point, different nucleation curves could be selected as shown in figure 3.5. To stay beneath the critical nucleation curve ($N_{s_{critical}} = \left(\frac{1}{2l}\right)^2$) the power of $\frac{1}{2l}$

was chosen to be 1, 1.3, 1.6 to stay in the green region under the critical curve and still have nucleation density increased by the reduction of size of micro-pillars or roughness spacing. These new curves are hypothetically chosen in order to provide an insight into the effect of change of nucleation density on overall resistance energy of the surface as a result of the variation of surface roughness size.

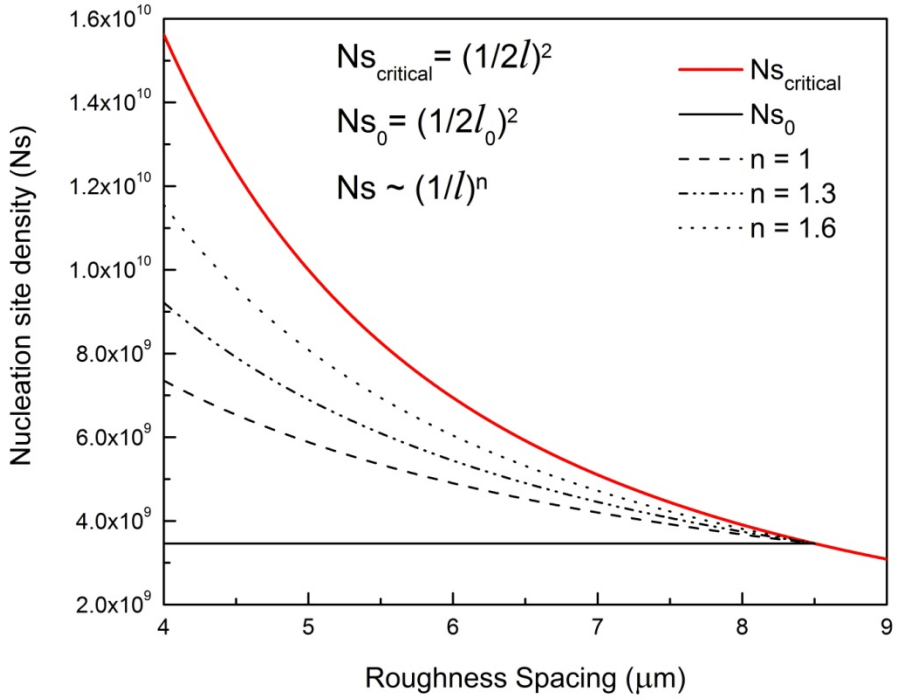

FIG. 4.5 Different hypothetical nucleation site density curves versus roughness spacing (l)

It can be seen in figure 4.6 that for different curves as roughness size decreases the overall resistance energy of the surface shows various behaviors. It is observed that as the rate of increase of nucleation sites rises (power n gets larger), by lowering the roughness size, the overall resistance energy of the surface could even increase ($n = 1.6$) despite the fact that the resistance energy of a single cell is decreasing (Fig.

4.3). In other words an increase in the number of nucleation sites leads to more tails of droplet in the cavity of first-tier structure. Therefore the overall resistance energy raises as a result of increase in the number of nucleation sites not an increase in resistance energy of a single cell.

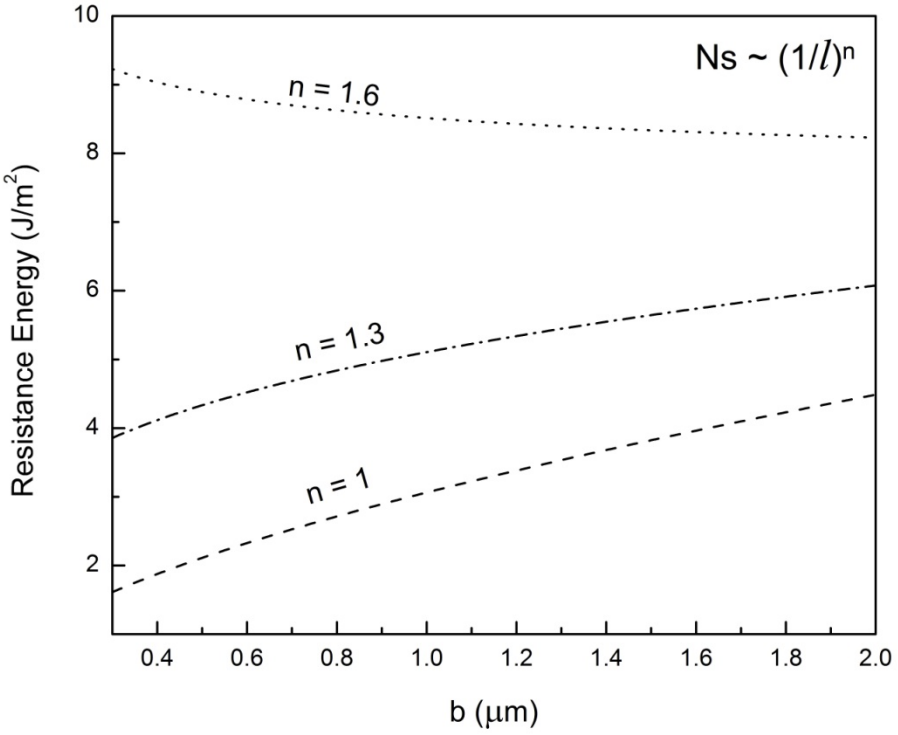

FIG. 4.6 Resistance energy of the entire surface versus size of first tier pillars for different hypotetical nucleation site density curves

CHAPTER 5

CONCLUSION

A theoretical analysis was carried out in order to optimize the first tier of superhydrophobic hierarchical surface. The optimization was done based on the minimization of the energy which needs to be overcome (resistance energy) in order for the tail of a condensate in the single cell (the cavity among four squarely positioned first-tier pillars) to achieve Wenzel state to Cassie state transition, i.e., expulsion of the entrapped tail of the droplet out of the cavities first-tier pillars. The second tier was assumed to be in nano-scale and by fixing the value of solid fraction while changing the size of the first tier the optimum size was calculated. It was shown that as the size of first tier approaches the nano-scale the resistance energy of the transition of the tail is lowered which confirms the necessity of having double tier structure both in nano-scale. Afterwards the effect of variation of nucleation site density due to the change of the size of roughness on the resistance energy of the entire surface was illustrated. It was mentioned that by fixing the nucleation site density as the size of roughness is lowered, the resistance energy of the entire surface decreases as seen for the analysis of the single cell. On the other hand it was clarified that by selecting different paths for the increase of nucleation sites as the size of first tier is lowered the resistance energy of the entire surface either increases or decreases based the rate of increase of nucleation sites. Therefore more experimental and theoretical analysis on the effect of surface roughness size on nucleation site density of the surface is required in order to predict the behavior of the surfaces during dropwise condensation.

REFERENCES

[1] E. Schmidt, W. Schurig, and W. Sellschopp, Technische Mechanik und Thermodynamik **1**, 53 (1930).

[2] Y.-T. Cheng and D. E. Rodak, Applied physics letters **86**, 144101 (2005).

[3] C. Dorrer and J. Rühe, Langmuir **23**, 3820 (2007).

[4] R. Narhe and D. Beysens, Physical review letters **93**, 076103 (2004).

[5] K. K. Varanasi, M. Hsu, N. Bhate, W. Yang, and T. Deng, Applied Physics Letters **95**, 094101 (2009).

[6] K. A. Wier and T. J. McCarthy, Langmuir **22**, 2433 (2006).

[7] J. B. Boreyko and C.-H. Chen, Physical review letters **103**, 184501 (2009).

[8] F.-C. Wang, F. Yang, and Y.-P. Zhao, Applied Physics Letters **98**, 053112 (2011).

[9] T. Liu, W. Sun, X. Sun, and H. Ai, Colloids and Surfaces A: Physicochemical and Engineering Aspects **414**, 366 (2012).

[10] K. Rykaczewski, A. T. Paxson, S. Anand, X. Chen, Z. Wang, and K. K. Varanasi, Langmuir **29**, 881 (2013).

[11] C. Lv, P. Hao, Z. Yao, Y. Song, X. Zhang, and F. He, Applied Physics Letters **103**, 021601 (2013).

[12] X. Chen, J. Wu, R. Ma, M. Hua, N. Koratkar, S. Yao, and Z. Wang, Advanced Functional Materials **21**, 4617 (2011).

[13] X. Ma, H. Ma, P. Cheng, S. Wang, Z. Lan, and B. Peng, Journal of Heat Transfer **134**, 021501 (2012).

[14] J. Cheng, A. Vandadi, and C.-L. Chen, Applied Physics Letters **101**, 131909 (2012).

[15] N. Miljkovic, R. Enright, Y. Nam, K. Lopez, N. Dou, J. Sack, and E. N. Wang, Nano letters **13**, 179 (2012).

[16] K. Rykaczewski, W. A. Osborn, J. Chinn, M. L. Walker, J. H. J. Scott, W. Jones, C. Hao, S. Yao, and Z. Wang, Soft Matter **8**, 8786 (2012).

[17] L. Gao and T. J. McCarthy, Langmuir **24**, 9183 (2008).

[18] B. Bhushan and Y. C. Jung, Progress in Materials Science **56**, 1 (2011).

[19] W. Barthlott and C. Neinhuis, Planta **202**, 1 (1997).

[20] C. Extrand, Langmuir **18**, 7991 (2002).

[21] C. Lv, C. Yang, P. Hao, F. He, and Q. Zheng, Langmuir **26**, 8704 (2010).

[22] G. McHale, N. Shirtcliffe, and M. Newton, Langmuir **20**, 10146 (2004).

[23] S. Moulinet and D. Bartolo, The European Physical Journal E **24**, 251 (2007).

[24] N. A. Patankar, Langmuir **19**, 1249 (2003).

[25] N. A. Patankar, Langmuir **20**, 8209 (2004).

[26] N. A. Patankar, Langmuir **20**, 7097 (2004).

[27] M. Reyssat and D. Quéré, The Journal of Physical Chemistry B **113**, 3906 (2009).

[28] Y. Xiu, L. Zhu, D. W. Hess, and C. Wong, The Journal of Physical Chemistry C **112**, 11403 (2008).

[29] P.-G. De Gennes, F. Brochard-Wyart, and D. Quéré, *Capillarity and wetting phenomena: drops, bubbles, pearls, waves* (Springer, 2004).

[30] D. Quéré, Reports on Progress in Physics **68**, 2495 (2005).

[31] D. Quéré, Nature Materials **1**, 14 (2002).

[32] A. Cassie, Discussions of the Faraday Society **3**, 11 (1948).

[33] A. Cassie and S. Baxter, Transactions of the Faraday Society **40**, 546 (1944).

[34] R. N. Wenzel, Industrial & Engineering Chemistry **28**, 988 (1936).

[35] R. N. Wenzel, The Journal of Physical Chemistry **53**, 1466 (1949).

[36] R. E. Johnson Jr and R. H. Dettre, The Journal of Physical Chemistry **68**, 1744 (1964).

[37] J. B. Boreyko and C.-H. Chen, Physical review letters **103**, 174502 (2009).

[38] G. Manukyan, J. Oh, D. Van Den Ende, R. Lammertink, and F. Mugele, Physical review letters **106**, 014501 (2011).

[39] N. Miljkovic, D. J. Preston, R. Enright, and E. N. Wang, ACS nano **7**, 11043 (2013).

[40] S. Chandra and C. Avedisian, Proceedings: Mathematical and Physical Sciences, 13 (1991).

[41] M. He *et al.*, Soft Matter **8**, 6680 (2012).

[42] I. A. Larmour, S. E. Bell, and G. C. Saunders, Angewandte Chemie **119**, 1740 (2007).

[43] C. W. Lo, C. C. Wang, and M. C. Lu, Advanced Functional Materials (2013).

[44] N. Miljkovic and E. N. Wang, MRS bulletin **38**, 397 (2013).